THE JOURNAL OF PHYSICAL CHEMISTRY Letters

Letter

A Chemical Understanding of the Limited Site-Specificity in Molecular Inner-Shell Photofragmentation

Ludger Inhester, Bart Oostenrijk, Minna Patanen, Esko Kokkonen, Stephen H. Southworth, Christoph Bostedt, Oksana Travnikova, Tatiana Marchenko, Sang-Kil Son, Robin Santra, Marc Simon, Linda Young, and Stacey L. Sorensen

J. Phys. Chem. Lett., **Just Accepted Manuscript** • DOI: 10.1021/acs.jpclett.7b03235 • Publication Date (Web): 14 Feb 2018

ACS Publications

The Journal of Physical Chemistry Letters is published by the American Chemical Society. 1155 Sixteenth Street N.W., Washington, DC 20036

A Chemical Understanding of the Limited Site-Specificity in Molecular Inner-Shell Photofragmentation

Ludger Inhester,[*,†,‡,††] Bart Oostenrijk,[*,¶,††] Minna Patanen,[§] Esko Kokkonen,[§] Stephen H. Southworth,[‖] Christoph Bostedt,[‖,⊥] Oksana Travnikova,[#] Tatiana Marchenko,[@,#] Sang-Kil Son,[†,‡] Robin Santra,[†,‡,△] Marc Simon,[#] Linda Young,[*,∇,‖] and Stacey L. Sorensen[*,¶]

†*Center for Free-Electron Laser Science, DESY, Notkestrasse 85, 22607 Hamburg, Germany*

‡*The Hamburg Centre for Ultrafast Imaging, Luruper Chaussee 149, 22761 Hamburg, Germany*

¶*Department of Physics, Lund University, Box 118, 221 00 Lund, Sweden*

§*Faculty of Science, Nano and Molecular Systems Research Unit, University of Oulu, BOX 3000, FIN-90014, Finland*

‖*Argonne National Laboratory, 9700 S. Cass Avenue, Lemont, IL 60439, USA*

⊥*Department of Physics, Northwestern University, 2145 Sheridan Road, Evanston, IL 60208, USA*

#*LCPMR, CNRS, Sorbonne Université, Laboratoire de Chimie Physique - Matière et Rayonnement, F-75005 Paris, France*

@*Synchrotron SOLEIL, l'Orme des Merisiers, Saint-Aubin, BP 48, F-91192 Gif-sur-Yvette Cedex, France*

△*Department of Physics, University of Hamburg, Jungiusstrasse 9, 20355 Hamburg, Germany*

∇*Department of Physics and James Franck Institute, The University of Chicago, Chicago, IL 60637, USA*

††*L.I. and B.O. contributed equally to this work.*

E-mail: ludger.inhester@cfel.de; bart.oostenrijk@sljus.lu.se; young@anl.gov; stacey.sorensen@sljus.lu.se

Abstract

In many cases fragmentation of molecules upon inner-shell ionization is very unspecific with respect to the initially localized ionization site. Often this finding is interpreted in terms of an equilibration of internal energy into vibrational degrees of freedom after Auger decay. Here we investigate the x-ray photofragmentation of ethyl trifluoroacetate upon core electron ionization at environmentally distinct carbon sites using photoelectron-photoion-photoion coincidence measurements and ab-initio electronic structure calculations. For all the 4 carbon ionization sites, the Auger decay weakens the same bonds and transfers the two charges to opposite ends of the molecule, which leads to a rapid dissociation into 3 fragments followed by further fragmentation steps. The lack of site-specificity is attributed to the character of the dicationic electronic states after Auger decay, instead of a fast equilibration of internal energy.

Graphical TOC Entry

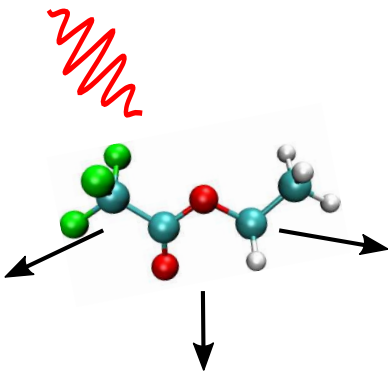

The ESCA molecule fragmenting after carbon inner-shell photoionization.

Understanding the consequences of photoabsorption, the dominant x-ray interaction with matter, is the basis of radiation damage and is crucial for experiments at modern synchrotron and free-electron laser light sources. Above the core electron ionization energy, the main photoabsorption process ejects an electron from a core orbital, leaving behind a localized inner-shell vacancy. The ensuing non-radiative decay is well characterized in atoms, but in molecules there is a competition between charge delocalization, Auger cascade, and Coulomb explosion where the underlying dissociation mechanism involves coupled nuclear and electronic motions.[1–7] In low-Z molecular systems, the inner-shell hole decays predominantly by Auger processes yielding electronic states with multiple valence holes. If the valence holes remain localized near the initial core hole, the fragmentation may be "site-selective" and thus provides a means to control chemical bond breakage. Site-selective photofragmentation has been extensively studied since the first observation by Eberhardt and colleagues where soft x-ray excitation of a core electron into an antibonding orbital in acetone resulted in prompt site-selective fragmentation.[8] Recently, fragmentation of a singly-ionized six-membered ring molecule produced by resonant inner shell excitation was compared with direct valence photoionization.[9] The preferential production of certain fragments was found to depend upon the population of the final states reached in the two situations, but a firm correlation between the excitation site and bond breakage could not be established.

More generally, x-ray photoionization proceeds via electron promotion into the continuum and relaxation by Auger decay. Experimentally this process has been studied[10–26] with electron-ion coincidence methods. Site-selectivity is obtained by exciting or ionizing atoms of different elements[10–12,22] or, for atoms of same elements, by using site-specific chemical shifts in a variety of medium-sized carbon[9,17,18,20,24,25] and silicon-containing[13,16,19] molecules. For most of these molecules only a relatively small fraction of the total ion yields is specific to the ionization site. The situation is drastically different for dicationic states reached after an Auger decay; in the classic case of CH_2ClBr at low internal energies (high Auger kinetic energy) a strong site-specific fragmentation was observed,[11] and the key role of the

internal energy—the excitation energy of the dicationic electronic state after Auger decay—was identified via Auger-photoion-photoion coincidence studies.

A theoretical understanding of the underlying mechanism is still at an early stage. The major role of the internal energy stems from the idea that fast conversion processes quickly transfer electronic excitation energy of the dication into vibrational degrees of freedom.[11] For example, the rich fragmentation patterns of the ring molecule thiophene (C_4H_4S) after ejection of a sulfur 2p electron were modeled using molecular dynamics assuming a statistical (thermal) distribution of the excitation energy into all vibrational degrees of freedom in the lowest electronic state of the dication.[27] In this model, the identities of the electronic states populated via Auger decay become irrelevant and the only important parameter determining the fragmentation remains the internal energy.

Other works that model x-ray photofragmentation also rely mainly on a statistical model,[21,23,27–30] as a theoretical description addressing molecular dissociation after x-ray ionization is challenging. Recently, this statistical model has been challenged by experimental observation that a site-specific fragmentation pattern persists at similar internal energy content[20,24] and that a seemingly minor substitution in a non-ionized site of the molecule can drastically change the fragmentation pattern.[23] Can we characterize the photoionization induced fragmentation dynamics with a purely statistical model, or is any memory of the core localization retained? How can we model such behavior?

Here we address these questions by studying both experimentally and theoretically the photofragmentation on the "ESCA" molecule, ethyl trifluoroacetate ($CF_3CO_2CH_2CH_3$), where the core ionization of the chemically distinct carbon atoms can be identified through their chemical shifts. Previously, Eland et al.[20] found a site-specific trend in fragmentation for some ion fragments (CF_3^+, CF_2^+, CF^+). By detecting ion fragments in coincidence with fast Auger electrons they showed that strong site-specificity occurs when one restricts oneself to low internal energies. In another work Auger spectra for specific ionization sites have been measured and analyzed.[31] Here we reinspect the photofragmentation of $CF_3CO_2CH_2CH_3$

with a focus on the fragmentation mechanisms associated with initial ionization sites using ion-ion coincidences and theoretical modelling of the observed trends.

Figure 1(a) shows the measured ion-mass spectra upon C1s ionization ($h\nu = 411\,\mathrm{eV}$), in coincidence with photoelectrons associated with each of the four ionization sites. The most abundant ion fragments are mono- and di-carbon hydride ion fragments (CH_n^+, $n = 0, \ldots, 3$; $C_2H_n^+$, $n = 2, \ldots, 5$), as well as carbon fluoride ions (CF_m^+, $m = 0, \ldots, 3$), and, much less abundant, carbon dioxide ions (CO_2^+) and fluorine ions (F^+). The unfragmented parent ion ($CF_3CO_2CH_2CH_3^{2+}$) and any doubly charged ions are not observed in the mass spectra. No ion fragments containing a CO_2 or CO group are observed, apart from a tiny contribution of CF_2CO^+. From the time-of-flight (ToF) correlation map (Figure S1), one can see that the fragment pairs CF_m^++CH_n^+ and CF_m^++$C_2H_n^+$ dominate the fragmentation channels, indicating that the bonds connecting the central CO_2 moiety (CO_2–CF_3 and CO_2–CH_2 bonds) break preferentially. Overall, the fragmentation pattern (Figure 1a) shows little site-dependence (83% of the ion yield unaffected by the initial ionization site).

Subtle site-dependent effects are illustrated by branching ratios for coincident fragment pairs containing CF_m^+ (Figure 1b) or CH_n^+/ $C_2H_n^+$ (Figure 1c). The series CF_3^+, CF_2^+, CF^+ indicates a decreasing degree of cleavage of C–F bonds as the ionization site moves further from the CF_3 group, as reported before.[20] A similar but weaker trend is observed for the ethyl and methyl fragments, where the production of $C_2H_n^+$ increases and that of CH_n^+ decreases as the ionization site moves away from the ethyl tail. These trends are also observed in the photoelectron spectrum coincident with ions and ion pairs (See section S2).

Details on the dissociation mechanism are revealed from the ion ToF correlation diagram, based on momentum conservation.[32,33] Since there is no significant difference in the ion-ion correlation maps for the different sites, we consider them together in the following analysis. For $ABC^{2+} \longrightarrow A^+ + B^+ + C$, the momentum of the undetected neutral fragment C is determined by momentum conservation from the momenta of the charged partner fragments A^+ and B^+. We assume that scission of a neutral fragment from a charged parent fragment

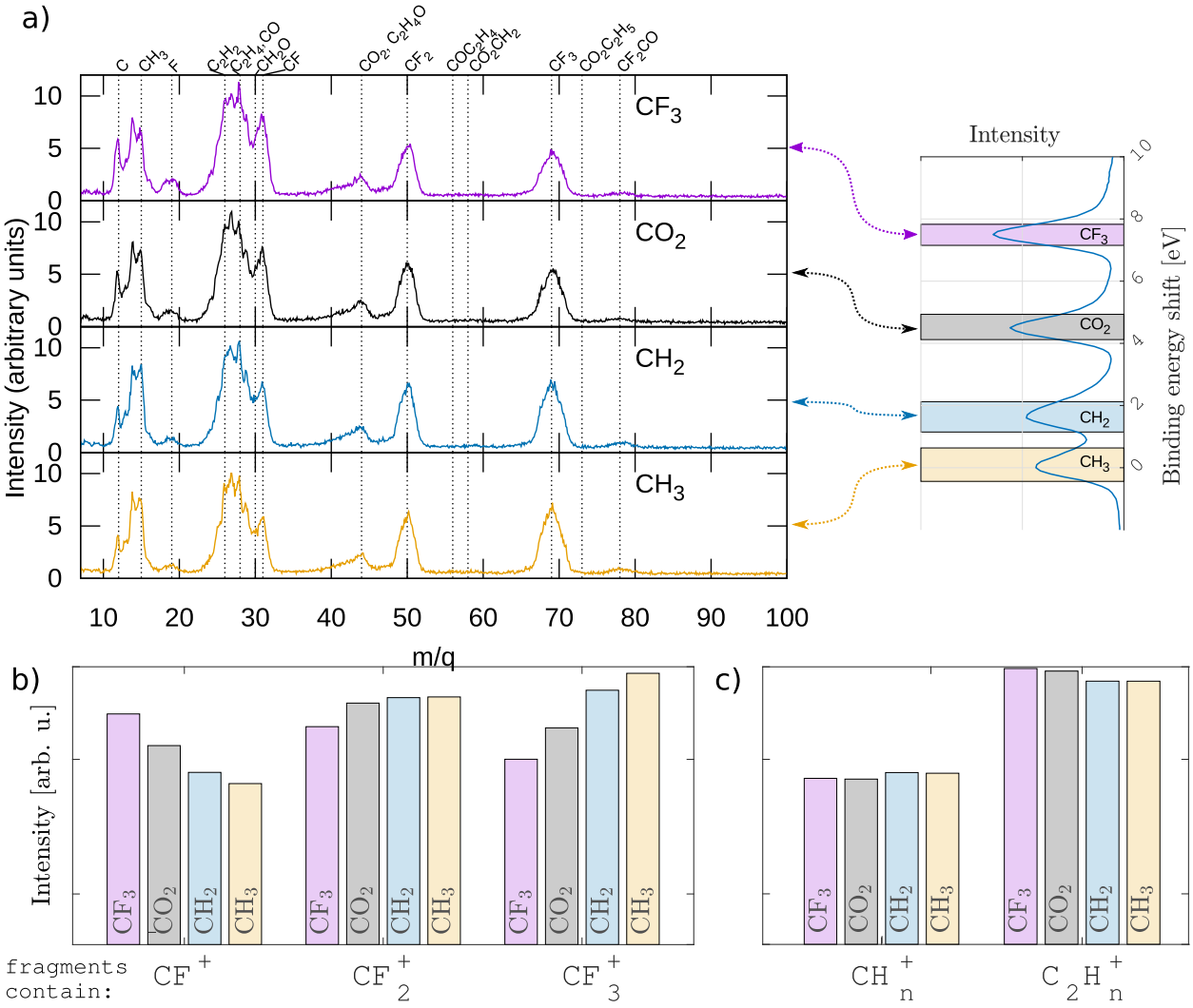

Figure 1: Ion-mass spectra in coincidence with photoelectrons from different carbon ionization sites(CF_3, CO_2, CH_2, CH_3). Top left: the ion-mass spectra after site selection, based on the electron energy. Top right: The photoelectron spectrum showing the chemical shift of each photoelectron. The shaded areas indicate the selection range used in the ion-mass spectra. Bottom: Branching ratios of fragment pairs containing a CF_m^+ (b) or CH_n^+ / $C_2H_n^+$ (c) fragment. The branching ratios are calculated from the measured abundance of double coincidence pairs that correspond to a photoelectron within the energy ranges shown in the top right.

does not produce a significant amount of momentum and in this case the momentum of the parent fragment is shared between neutral and charged products at the ratio of their masses. For a concerted three particle break-up into two charged particles and a neutral partner, the two charged fragments gain opposite momenta and the neutral fragment is left behind with little momentum.

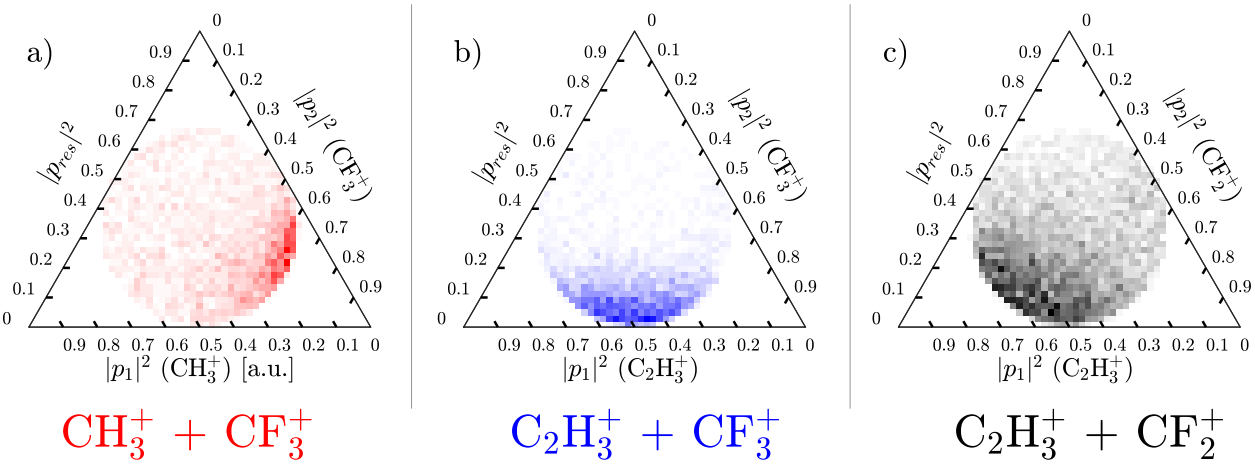

Figure 2: The momentum sharing map of two fragment pairs and the residual momentum coincident with one carbon inner-shell photoelectron (any ionization site): $CH_3^+ + CF_3$ (a), $C_2H_3^+ + CF_3^+$ (b) and $C_2H_3^+ + CF_2^+$ (c). Each of three axis represents the absolute momentum squared, normalized to the sum of absolute momenta squared $\sum_n |\vec{p_n}|^2$.

Figure 2 displays momentum correlations in triangular Dalitz plots,[34] where the absolute momenta of two coincident fragments are plotted, normalized by the sum of the absolute values of all momenta. This momentum sum indicates the missing momentum of undetected neutral fragments, since the total momenta of all fragments should be close to zero. For three specific fragment pairs, the Dalitz plots give a crucial insight into the fragmentation mechanism. Figure 2b shows the dominantly detected fragment pair, $C_2H_3^+ + CF_3^+$, indicating an equal sharing of momenta on both ions, resulting in a small residual momentum. This indicates that the momenta of the undetected CO_2 fragment and that of evaporated hydrogens are very small. Because CO_2 is the central moiety in the molecule, we infer that the two charged fragments fly off simultaneously in opposite directions due to Coulomb repulsion, leaving the remaining CO_2 fragment at rest.

The momentum sharing mechanism of the channels with CF_3^+ and CH_3^+ as final charged products is very different, as shown in Figure 2a. In the Dalitz plot one clearly sees a tendency for unequal momentum sharing. The absolute momentum of CH_3^+ is much lower that of the corresponding CF_3^+ fragment partner. We ascribe the residual momentum to the undetected neutral methylene that is created during a secondary break-up of $C_2H_n^+$, after the initial break-up of the ESCA molecule.

A similar observation is found for fluorine loss, $CF_3^+ \longrightarrow CF_2^+ + F$, in Figure 2c. There is a significant amount of residual momentum at the expense of momentum in the detected CF_2^+ fragment. Following the same argument, the lost momentum is likely to be carried away by the undetected fluorine atom that dissociates from CF_3^+ after the initial break-up of the molecule.

The momentum correlations discussed above strongly indicate an initial concerted break-up into $C_2H_n^+$ and CF_3^+ fragments and a neutral CO_2 molecule. Afterwards, either charged fragment can further break up. The ethyl fragment can split into two methyl/methylene fragments, where one carries the charge, and the trifluoromethyl fragment can lose fluorine atoms. In summary, the dominant break-up scheme is

$$\begin{aligned} C_2H_5{-}CO_2{-}CF_3^{2+} &\longrightarrow C_2H_n^+ + CO_2 + CF_3^+ + (5{-}n)\,H \\ \text{in some cases: } C_2H_n^+ &\longrightarrow CH_m^+ + CH_{n-m} \\ \text{in some cases: } CF_3^+ &\longrightarrow CF_m^+ + (3{-}m)\,F. \end{aligned}$$

This break-up scheme holds consistently for all four carbon ionization sites.

Since the site-selectivity of the fragmentation is so low, one might be tempted to think that after Auger decay the internal energy in the dicationic molecule has equilibrated among the molecular degrees of freedom resulting in a similar fragmentation path from each initial C 1s vacancy such that any memory of the initial ionization site is lost. However, the initial

simultaneous bond rupture and the strict sequence of bond breaking strongly indicate that the creation of CF_3^+ and $CH_2CH_3^+$ takes place directly after the Auger decay, leaving little time for equilibration of the internal energy. At the same time, the observed small site-specific fragmentation trends demonstrate that the memory on where the core-ionization happened survives at least to a certain degree until the onset of secondary break-up. Thus, our observations indicate that the bond breakage of the molecule is not governed by a statistical mechanism in which the internal energy is equilibrated over the vibrational degrees of freedom prior to fragmentation. Instead, we think that the fragmentation is determined by the specific character of the electronic states populated after Auger decay as has been suggested in Refs. 9,20,24.

To investigate this idea theoretically, we now consider the fragmentation dynamics in the final states after Auger decay. For simplicity, we neglect double Auger/shake-off processes and focus on the Auger process leading to two holes in the valence shells, which comprise the dominant fraction ($\simeq 90\%$) of created ions. From molecular dynamics calculations in the core ionized states we verified that the molecule does not undergo significant geometry rearrangements within the lifetime of the core hole ($\simeq 10\,\mathrm{fs}$) (see section S5). In the two-valence-hole state after Auger decay molecular bonds are weakened significantly. Additionally, the molecule now carries two charges, which leads to strong Coulomb repulsion of charged parts in the molecule. To investigate the trends for dissociation in the different two-valence-hole states, we inspect the character of molecular bonds and how they are weakened through Auger decay. We calculate the Auger rates for the many involved final dicationic electronic states employing a methodology that is sufficiently accurate to describe the relevant characteristics (see section S4). For these states, we evaluate the bond orders of the chemical bonds[35–37] and weight them with their respective Auger branching ratios. Calculation details are given in the Methods section.

Figure 3 shows the histogram of bond order values after Auger decay for each selected bond in the molecule. The atom labeling is shown on top of the figure. The different panels

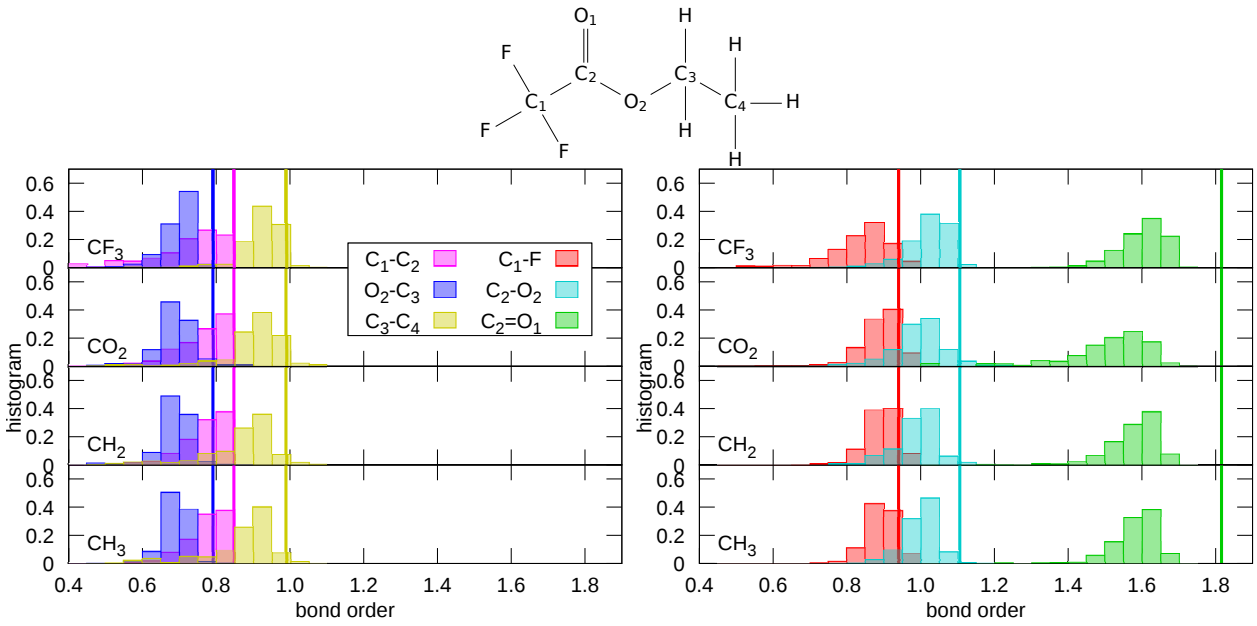

Figure 3: Bond order distribution after Auger decay at a given ionization site for specific bonds (56% anti-anti, 44% anti-gauche conformer). The labeling of the bonds is given in the structural formula above. The vertical lines in the plot indicate the bond order value of the neutral state.

indicate the different core ionization sites. The vertical lines indicate the bond order value for the neutral state. As can be seen, for the neutral electronic configuration the bond order is $\simeq 1$ for bonded atom pairs. The $C_2{=}O_1$ double bond is the strongest with a value of $\simeq 1.8$. The bond connecting the fluoromethyl group and the carbonyl group ($C_1{-}C_2$) and the oxygen-methylene bond ($O_2{-}C_3$) are the weakest with bond orders of $\simeq 0.85$ and $\simeq 0.80$, respectively.

For the two-valence-hole states populated after Auger decay, the bond order distribution indicates that all considered are weakened compared to the neutral state. Overall, no strong signal of ionization site-specificity is seen. The oxygen-methylene ($O_2{-}C_3$) and the fluoromethyl-carbonyl ($C_1{-}C_2$) bonds remain the weakest. The methylene-methyl bond ($C_3{-}C_4$) is less affected. Its bond order peaks at 0.9 and shows a distribution to weaker bonds. For the CH_3 and CH_2 core holes the distribution is slightly shifted to lower values compared to the CO_2 and CF_3 core holes. The $C_1{-}F$ bond is rather weakly affected and peaked around 0.9. There is a clear trend for a weaker bond with ionization on the CF_3 site.

The bond C_2-O_2 is weakly affected and its distribution is centered around 1 for all ionization sites. The double bond $C_2=O_1$ is strongly shifted but maintains its strong double-bond character (bond order $\gtrapprox 1.5$).

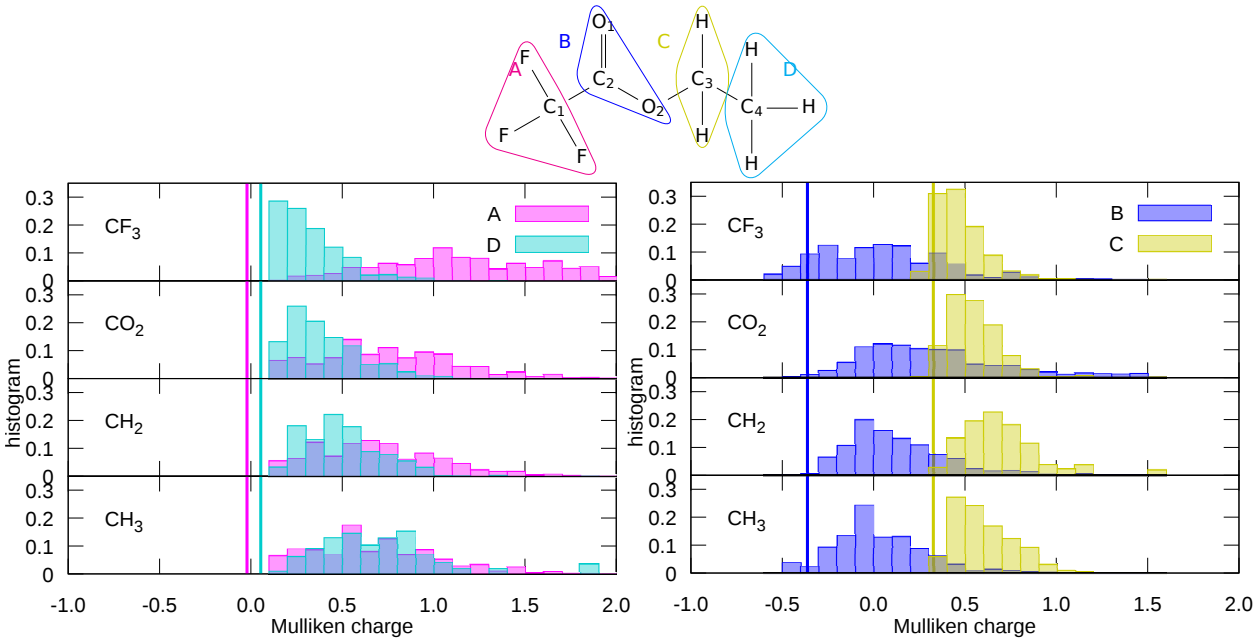

Figure 4: Distribution of Mulliken charges of constituents of the molecule after Auger decay at a given ionization site (56% anti-anti, 44% anti-gauche conformer). The moieties of A, B, C, and D are defined in the structural formula above. The vertical lines indicate the Mulliken charge for the neutral state.

In order to understand the trends in charge distribution among the different molecular fragments we inspect the distribution of Mulliken charges after Auger decay as shown in Figure 4. The different panels describe the charge distributions for the different ionization sites. Auger decay increases the charge of all moieties and the two charges are broadly distributed over the molecule confirming previous observations.[31] For all ionization sites, the strongest shift in charge distribution appears in the fluoromethyl part, A, which also carries the largest charge regardless of ionization site. In contrast, the CO_2 part, B, stays neutral with values of -0.5 to 0.5. The charge of the methylene and methyl moieties, C and D, is distributed in the range 0.0–1.0, respectively.

As can be seen from this analysis, the most abundant fragments as well as the low site-

specificity are explained by the trends in the bond order distribution in the final dicationic states of the molecule. For all 4 ionization sites the weakest bonds, C_1-C_2 and O_2-C_3, break. The bonds of intermediate strength, C_3-C_4 and C_1-F, break only in some fragmentation channels. The positive charge in the molecule is distributed in such a way that both CF_3 and CH_2CH_3 fragments carry away a positive charge, and the CO_2 fragment remains neutral. In agreement with the distribution of bond order values, the site-specificity in the fragmentation is low. The observed site-specific trends, the larger abundance of CF^+ at the expense of $CF_3{}^+$ fragments for ionization on CF_3 and the more likely breaking of the C_3-C_4 for ionization on CH_2 or CH_3, can be explained by the site-specific characteristics of the bond order distributions. We note that, if one focuses on a specific range of internal energies (e.g., by filtering for specific Auger energies) stronger site-specificity in the fragmentation may be seen (see section S6), as recently observed.[20,24] It should be noted that double Auger/shake-off processes neglected in our theoretical model may have an overall contribution of 10% or more.[38] The possibility exists that these processes might have a role on the site-specificity of photofragmentation.

In summary, we have measured the photofragmentation of ethyl trifluoroacetate using photoelectron-photoion-photoion coincidence measurements after carbon 1s ionization and analyzed the fragmentation mechanisms for the dominant fragmentation channels. We find that fragmentation is largely unspecific to the ionization site. Because the initial fragmentation takes place quickly after Auger decay, it is very unlikely that the loss of site-specificity is due to equilibration of the internal energy in the electronic ground state, even if molecular dynamics simulations with internal energy as a determining parameter have successfully modeled x-ray photofragmentation of some molecules.[27,28] Here we have used ab-initio electronic structure methods to investigate all the Auger decay channels for each of the four carbon ionization sites. A bond order analysis for all the final electronic states reproduces all of the trends shown in the ion mass spectra. In particular, for all initial ionization sites the Auger decay populates dicationic electronic states in which the same specific bonds are

weakened. Therefore, the fragmentation is not strongly correlated with the initial ionization site. Additionally, we can demonstrate that the small site-specific trends in the experimental ion yields are qualitatively rationalized by the calculated bond order distribution after Auger decay. We conclude that it is not the internal energy left in the molecule but the character of the two-valence hole states populated through Auger decay that essentially determines the fragmentation pattern. Our theoretical approach may present a route to efficient modeling of x-ray photofragmentation of molecules, which is complementary to approaches that do not take into account the specificity of the excited electronic states populated after Auger decay.[21,23,27–30]

Methods

Experimental methods

The experiment was carried out at the PLEIADES beamline at the SOLEIL synchrotron radiation facility in Saint Aubin, France,[39] using the EPICEA spectrometer described elsewhere.[40–43] In short, the EPICEA setup combines a double-toroidal electron-energy analyzer and an ion ToF spectrometer, both equipped with time- and position-sensitive detectors. The setup was used in coincidence mode, where the analyzer acceptance was maximized for an energy resolution that is sufficient to resolve the chemically-shifted C 1s peaks in the XPS spectrum; the pass energy of the analyzer was set to 120 eV, allowing to detect all four C 1s electrons simultaneously. A three-dimensional focusing ion ToF spectrometer detects molecular fragment ions using a delay-line anode detector. The ion extraction potential is triggered by detection of an electron, and multiple ions may be detected for each electron start signal. The relatively low electron collection efficiency ($\simeq 2\%$[44]) results in the detection of less electrons than ions, contributing to the measurement of false coincidences (see supporting information section 1 for further discussion). We filter the data for those coincidence events in which ions are detected with exactly one carbon 1s photoelectron. The

measurements were carried out at 411 eV with a photon bandwidth of 40 meV. The resulting electron rate was kept at 25 Hz.

The ion signals were filtered according to the radius of the electron signal, after correction for the angular variation of the detection radius, due to slight non-uniformities in the electrostatic field and the multi-channel plates (MCP) in the detector. The conversion of radial position to electron kinetic energy was performed as suggested in Ref. 44. The position-sensitive detection allows to measure ion impact positions and to determine the ion's three-dimensional momentum.

In a previous study using a magnetic bottle spectrometer,[20] the emitted Auger electrons, photoelectrons, and ions are detected in coincidence, allowing for the selection of certain Auger transitions. The EPICEA setup, used in the present experiment, allows efficient simultaneous detection of multiple fragment ions in coincidence with a photoelectron, regardless of the preceding Auger transition. Moreover, the coincidence position-sensitive ion pair detection allows us to determine the ion three-dimensional linear momentum and kinetic energy, which reveals the sequence of ionic breakup.

Computational methods

Geometry optimization

Ethyl trifluoroacetate is famous as a textbook example of a molecule with four carbon atoms having distinct chemical shifts.[45] It is also known as the *ESCA* (Electron Spectroscopy for Chemical Analysis) molecule, celebrating the concept of Kai Siegbahn and coworkers to utilize core-level chemical shifts for conducting chemical analysis.[46] There exist two conformers of $CF_3CO_2CH_2CH_3$, one with C_s symmetry (anti-anti conformer) and the other with C_1 symmetry (anti-gauche conformer) that appear with 56% and 44% in equilibrium, respectively.[47] This population ratio of conformers is considered for all calculations. The geometries of the two conformers that are used for the present calculations are obtained[47] from a MP2 geometry optimization employing the 6-311G++(d,p) basis set using GAMESS[48] and are

illustrated in Figure S2.

Calculation of Auger decay rates

With the XMOLECULE[49,50] toolkit we calculate the electronic structure of $CF_3CO_2CH_2CH_3$ employing the 6-31G** basis set[51,52] and the Hartree-Fock-Slater electronic structure model. For efficient Gaussian integral evaluation we employ the LIBCINT[53] integral library. For each of the four carbon core hole configurations in the two conformers, we perform electronic structure calculations by optimizing the molecular orbitals in the presence of the respective core hole. To calculate Auger decay rates we employ the methods described in Ref. 50. To this end the molecular orbitals expressed in the 6-31G** basis are projected onto the minimal basis set,[54] in which the atomic radial matrix elements are provided by the XATOM toolkit.[55]

To describe the final doubly-ionized electronic states after Auger decay, we employ configuration interaction (CI) calculations using orbitals optimized for the doubly-ionized ground state (employing a finite temperature distribution for the electronic occupation numbers of $k_bT = 0.1\,\mathrm{eV}$), taking into account the configuration space spanned by all two-valence-hole combinations. The Auger rates for the individual CI states $|\Psi_f\rangle$ are obtained by projecting them onto the two-valence-hole space within the core-hole-optimized orbital set. Employing this projection, the Auger rate for a final state $|\Psi_f\rangle$ from the initial core hole state $|\Psi_i\rangle$ is calculated by

$$\Gamma_{i\to f} = \left| \sum_{a<b} \langle \Psi_f | c_b c_a c_c^\dagger | \Psi_i \rangle \, \langle \phi_c \phi_\epsilon | \frac{1}{r_{12}} | \phi_a \phi_b \rangle \right|^2 . \quad (1)$$

The sum in Eq. 1 runs over all valence orbitals pairs ϕ_a and ϕ_b. The operators c_a, c_b and c_c are annihilation operators for electrons in the valence orbitals a, b, and the core orbital c, respectively. The matrix element $\langle \phi_c \phi_\epsilon | 1/r_{12} | \phi_a \phi_b \rangle$ is the electron interaction integral of the two valence electrons ϕ_a and ϕ_b with the continuum electron ϕ_ϵ and the core electron ϕ_c. In our approach, this two-electron integral is evaluated using the one-center approximation.[50]

Because we use different sets of orbitals for the initial state $|\Psi_i\rangle$ and the final states $|\Psi_f\rangle$, evaluation of Eq. 1 involves an overlap of the CI state $|\Psi_f\rangle$ with the two-valence-hole

configurations $c_b c_a c_c^\dagger|\Psi_i\rangle$ expressed with core-hole state optimized orbitals. For this overlap we obtain a projection norm,

$$\sum_f |\langle\Psi_f|c_b c_a c_c^\dagger|\Psi_i\rangle|^2, \tag{2}$$

that is in the range of 0.7–0.8 throughout all two-valence-hole configurations a,b. This value shows that the two Fock-subspaces described by the two orbital sets are largely overlapping and only a small quantity of a two-valence-hole configuration cannot be assigned to a final CI vector. We have validated our electronic structure method by comparing calculated core level shifts and Auger spectra with measurements (see supporting information section S3).

Bond Order Analysis

The bond order is a quantity that indicates how many bonding electrons are involved in the respective molecular bond between two atoms and is therefore a measure for the bond strength. To estimate bond order values, we perform Mayer's bond order analysis[56] based on the above mentioned electronic structure calculations for each final electronic state after Auger decay. In detail, from the one-particle density matrix D for each CI vector we calculate the bond order values between neighboring atoms A and B,

$$B_{AB} = \sum_{\mu \text{ on atom A}} \sum_{\nu \text{ on atom B}} (DS)_{\mu\nu}(DS)_{\nu\mu}, \tag{3}$$

where S is the overlap matrix of the basis functions and the sum μ and ν runs over basis functions centered on atom A and atom B, respectively. By weighting the bond order value with the Auger decay branching ratio we obtain a distribution of bond order values after the Auger decay from a specific core hole.

Acknowledgement

We thank Yi-Jen Chen for her careful reading of the manuscript. Work by MP was supported by Academy of Finland (decision no. 296338). Work by SHS, CB and LY was supported by the US Department of Energy, Office of Science, Basic Energy Science, Chemical Sciences, Geosciences and Biosciences Division under contract no. DE-AC02-06CH11357.

Supporting Information Available

The supplementary information contains the ToF correlation map, ion-selected photoelectron spectra, an illustration of the conformer geometries used for the calculations, a comparison of calculated core level shifts and Auger spectra with experimental data, an analysis of core ionized state molecular dynamics calculations, and a discussion of the bond order distribution as a function of internal energy. This material is available free of charge via the Internet at `http://pubs.acs.org/`.

References

(1) Erk, B.; Rolles, D.; Foucar, L.; Rudek, B.; Epp, S. W.; Cryle, M.; Bostedt, C.; Schorb, S.; Bozek, J.; Rouzee, A. et al. Ultrafast Charge Rearrangement and Nuclear Dynamics upon Inner-Shell Multiple Ionization of Small Polyatomic Molecules. *Phys. Rev. Lett.* **2013**, *110*, 053003.

(2) Travnikova, O.; Kimberg, V.; Flammini, R.; Liu, X.-J.; Patanen, M.; Nicolas, C.; Svensson, S.; Miron, C. On Routes to Ultrafast Dissociation of Polyatomic Molecules. *J. Phys. Chem. Lett.* **2013**, *4*, 2361–2366.

(3) Li, Z.; Vendrell, O.; Santra, R. Ultrafast Charge Transfer of a Valence Double Hole in Glycine Driven Exclusively by Nuclear Motion. *Phys. Rev. Lett.* **2015**, *115*, 143002.

(4) Picón, A.; Lehmann, C. S.; Bostedt, C.; Rudenko, A.; Marinelli, A.; Osipov, T.; Rolles, D.; Berrah, N.; Bomme, C.; Bucher, M. et al. Hetero-site-specific X-ray Pump-probe Spectroscopy for Femtosecond Intramolecular Dynamics. *Nat. Commun.* **2016**, *7*, 11652.

(5) Nagaya, K.; Motomura, K.; Kukk, E.; Fukuzawa, H.; Wada, S.; Tachibana, T.; Ito, Y.; Mondal, S.; Sakai, T.; Matsunami, K. et al. Ultrafast Dynamics of a Nucleobase Analogue Illuminated by a Short Intense X-ray Free Electron Laser Pulse. *Phys. Rev. X* **2016**, *6*, 021035.

(6) Rudenko, A.; Inhester, L.; Hanasaki, K.; Li, X.; Robatjazi, S. J.; Erk, B.; Boll, R.; Toyota, K.; Hao, Y.; Vendrell, O. et al. Femtosecond Response of Polyatomic Molecules to Ultra-intense Hard X-rays. *Nature* **2017**, *546*, 129–132.

(7) Travnikova, O.; Sisourat, N.; Marchenko, T.; Goldsztejn, G.; Guillemin, R.; Journel, L.; Céolin, D.; Ismail, I.; Lago, A. F.; Püttner, R. et al. Subfemtosecond Control of Molecular Fragmentation by Hard X-Ray Photons. *Phys. Rev. Lett.* **2017**, *118*, 213001.

(8) Eberhardt, W.; Sham, T. K.; Carr, R.; Krummacher, S.; Strongin, M.; Weng, S. L.; Wesner, D. Site-Specific Fragmentation of Small Molecules Following Soft-X-Ray Excitation. *Phys. Rev. Lett.* **1983**, *50*, 1038–1041.

(9) Bolognesi, P.; Kettunen, J. A.; Cartoni, A.; Richter, R.; Tosic, S.; Maclot, S.; Rousseau, P.; Delaunay, R.; Avaldi, L. Site- and State-Selected Photofragmentation of 2Br-Pyrimidine. *Phys. Chem. Chem. Phys.* **2015**, *17*, 24063–24069.

(10) Schmelz, H.; Reynaud, C.; Simon, M.; Nenner, I. Site-selective Fragmentation in Core-excited Bromo-chloro-alkanes [$Br(CH_2)_nCl$]. *J. Chem. Phys.* **1994**, *101*, 3742–3749.

(11) Miron, C.; Simon, M.; Leclercq, N.; Hansen, D. L.; Morin, P. Site-Selective Photochemistry of Core Excited Molecules: Role of the Internal Energy. *Phys. Rev. Lett.* **1998**, *81*, 4104–4107.

(12) Le Guen, K.; Ahmad, M.; Céolin, D.; Lablanquie, P.; Miron, C.; Penent, F.; Morin, P.; Simon, M. Influence of Formation Path on the $CH_2BrCl_2^+$ Dissociation Dynamics. *J. Chem. Phys.* **2005**, *123*, 084302–084311.

(13) Nagaoka, S.; Tamenori, Y.; Hino, M.; Kakiuchi, T.; Ohshita, J.; Okada, K.; Ibuki, T.; Suzuki, I. Site-specific Fragmentation Caused by Si : 1s Core-level Photoionization of $F_3SiCH_2CH_2Si(CH_3)_3$ vapor. *Chem. Phys. Lett.* **2005**, *412*, 459–463.

(14) Fukuzawa, H.; Prümper, G.; Nagaoka, S.-I.; Ibuki, T.; Tamenori, Y.; Harries, J.; Liu, X.; Ueda, K. Site-specific Fragmentation Following F 1s Photoionization of Free CF_3SF_5 Molecules Studied by Electron–Ion Coincidence Spectroscopy. *Chem. Phys. Lett.* **2006**, *431*, 253–256.

(15) Mocellin, A.; Wiesner, K.; Sorensen, S. L.; Miron, C.; Le Guen, K.; Céolin, D.; Simon, M.; Morin, P.; Machado, A. B.; Björneholm, O. et al. Site Selective Dissociation Upon Core Ionization of Ozone. *Chem. Phys. Lett.* **2007**, *435*, 214–218.

(16) Nagaoka, S.; Prümper, G.; Fukuzawa, H.; Hino, M.; Takemoto, M.; Tamenori, Y.; Harries, J.; Suzuki, I. H.; Takahashi, O.; Okada, K. et al. Electron-ion-ion Triple-Coincidence Spectroscopic Study of Site-specific Fragmentation Caused by Si : 2p Core-level Photoionization of $F_3SiCH_2CH_2Si(CH_3)_3$ Vapor. *Phys. Rev. A* **2007**, *75*, 020502.

(17) Itälä, E.; Kukk, E.; Ha, D.; Granroth, S.; Caló, A.; Partanen, L.; Aksela, H.; Aksela, S. Fragmentation Patterns of Doubly Charged Acrylonitrile Molecule Following Carbon Core Ionization. *J. Chem. Phys.* **2009**, *131*, 114314.

(18) Itälä, E.; Ha, D. T.; Kooser, K.; Huels, M. A.; Rachlew, E.; Nõmmiste, E.; Joost, U.; Kukk, E. Molecular Fragmentation of Pyrimidine Derivatives Following Site-selective Carbon Core Ionization. *J. Electron Spectrosc. Relat. Phenom.* **2011**, *184*, 119–124.

(19) Nagaoka, S.; Fukuzawa, H.; Prümper, G.; Takemoto, M.; Takahashi, O.; Yamaguchi, K.; Kakiuchi, T.; Tabayashi, K.; Suzuki, I. H.; Harries, J. R. et al. A Study to Control

Chemical Reactions Using Si:2p Core Ionization: Site-Specific Fragmentation. *J. Phys. Chem. A* **2011**, *115*, 8822–8831.

(20) Eland, J. H. D.; Linusson, P.; Mucke, M.; Feifel, R. Homonuclear Site-specific Photochemistry by an Ion–Electron Multi-Coincidence Spectroscopy Technique. *Chem. Phys. Lett.* **2012**, *548*, 90–94.

(21) Ha, D. T.; Wang, Y.; Alcamí, M.; Itälä, E.; Kooser, K.; Urpelainen, S.; Huels, M. A.; Kukk, E.; Martín, F. Fragmentation Dynamics of Doubly Charged Methionine in the Gas Phase. *J. Phys. Chem. A* **2014**, *118*, 1374–1383.

(22) Levola, H.; Itälä, E.; Schlesier, K.; Kooser, K.; Laine, S.; Laksman, J.; Ha, D. T.; Rachlew, E.; Tarkanovskaja, M.; Tanzer, K. et al. Ionization-site Effects on the Photofragmentation of Chloro- and Bromoacetic Acid Molecules. *Phys. Rev. A* **2015**, *92*, 063409.

(23) Itälä, E.; Levola, H.; Ha, D. T.; Kooser, K.; Rachlew, E.; Kukk, E. Photofragmentation of Serine Following C 1s Core Ionization-Comparison with Cysteine. *J. Phys. Chem. A* **2016**, *120*, 5419–5426.

(24) Zagorodskikh, S.; Eland, J. H. D.; Zhaunerchyk, V.; Mucke, M.; Squibb, R. J.; Linusson, P.; Feifel, R. Mechanisms of Site-specific Photochemistry Following Core-shell Ionization of Chemically Inequivalent Carbon Atoms in Acetaldehyde (ethanal). *J. Chem. Phys.* **2016**, *145*, 124302.

(25) Nagaoka, S.; Kakiuchi, T.; Ohshita, J.; Takahashi, O.; Hikosaka, Y. Site-Specific Electron-Relaxation Caused by Si:2p Core-Level Photoionization: Comparison between $F_3SiCH_2CH_2Si(CH_3)_3$ and $Cl_3SiCH_2CH_2Si(CH_3)_3$ Vapors by Means of Photoelectron Auger Electron Coincidence Spectroscopy. *J. Phys. Chem. A* **2016**, *120*, 9907–9915.

(26) Lago, A. F.; Januário, R. D.; Cavasso Filho, R.; Simon, M.; Dávalos, J. Z. Photoionization and Ionic Dissociation of the C_3H_3NS Molecule Induced by Soft X-ray near the C1s Edge. *J. Mass Spectrom.* **2017**, *52*, 657–663.

(27) Kukk, E.; Ha, D. T.; Wang, Y.; Piekarski, D. G.; Diaz-Tendero, S.; Kooser, K.; Itälä, E.; Levola, H.; Alcamí, M.; Rachlew, E. et al. Internal Energy Dependence in X-ray-induced Molecular Fragmentation: An Experimental and Theoretical Study of Thiophene. *Phys. Rev. A* **2015**, *91*, 043417.

(28) Yamazaki, K.; Nakamura, T.; Niitsu, N.; Kanno, M.; Ueda, K.; Kono, H. Communication: Two-step Explosion Processes of Highly Charged Fullerene Cations C_{60}^{q+} (q = 20–60). *J. Chem. Phys.* **2014**, *141*, 121105.

(29) Herve du Penhoat, M.-A.; Kamol Ghose, K.; Gaigeot, M.-P.; Vuilleumier, R.; Fujii, K.; Yokoya, A.; Politis, M.-F. Investigation of the Fragmentation of Core-Ionised Deoxyribose: A Study as a Function of the Tautomeric Form. *Phys. Chem. Chem. Phys.* **2015**, *17*, 32375–32383.

(30) Nagaya, K.; Motomura, K.; Kukk, E.; Takahashi, Y.; Yamazaki, K.; Ohmura, S.; Fukuzawa, H.; Wada, S.; Mondal, S.; Tachibana, T. et al. Femtosecond Charge and Molecular Dynamics of I-Containing Organic Molecules Induced by Intense X-Ray Free-Electron Laser Pulses. *Faraday Discuss.* **2016**, *194*, 537–562.

(31) Iwayama, H.; Sisourat, N.; Lablanquie, P.; Penent, F.; Palaudoux, J.; Andric, L.; Eland, J.; Bucar, K.; Zitnik, M.; Velkov, Y. et al. A Local Chemical Environment Effect in Site-specific Auger Spectra of Ethyl Trifluoroacetate. *J. Chem. Phys.* **2013**, *138*, 024306.

(32) Eland, J. H. D. Dynamics of Fragmentation Reactions from Peak Shapes in Multiparticle Coincidence Experiments. *Laser Chem.* **1991**, *11*, 259–263.

(33) Simon, M.; Lebrun, T.; Martins, R.; Desouza, G. G. B.; Nenner, I.; Lavollée, M.; Morin, P. Multicoincidence Mass-Spectrometry Applied to Examethyldisilane Excited around the Si 2p Edge. *J. Phys. Chem.* **1993**, *97*, 5228–5237.

(34) Dalitz, R. H. CXII. On the Analysis of τ-meson Data and the Nature of the τ-meson. *The London, Edinburgh, and Dublin Philosophical Magazine and Journal of Science* **1953**, *44*, 1068–1080.

(35) Somogyi, A.; Gömöry, A.; Vékey, K.; Tamás, J. Use of Bond Orders and Valences for the Description and Prediction of Primary Fragmentation Processes. *Org. Mass Spectrom.* **1991**, *26*, 936–938.

(36) Mayer, I.; Gömöry, A. Predicting Primary Mass Spectrometric Cleavages: a 'Quasi-Koopmans' ab initio Approach. *Chem. Phys. Lett.* **2001**, *344*, 553–564.

(37) Takahashi, O.; Mitani, M.; Joyabu, M.; Saito, K.; Iwata, S. Theoretical Studies on the Molecular Dependence of the Bond Dissociation After the Core Excitations $CH_3OCO(CH2)_nCN, n = 0, 1, 2$. *J. Electron Spectrosc. Relat. Phenom.* **2001**, *120*, 137–148.

(38) Roos, A. H.; Eland, J. H. D.; Andersson, J.; Zagorodskikh, S.; Singh, R.; Squibb, R. J.; Feifel, R. Relative Extent of Double and Single Auger Decay in Molecules Containing C, N and O Atoms. *Phys. Chem. Chem. Phys.* **2016**, *18*, 25705–25710.

(39) SOLEIL website. `http://www.synchrotron-soleil.fr/Recherche/LignesLumiere/PLEIADES`, access date: 10.01.2018.

(40) Miron, C.; Simon, M.; Leclercq, N.; Morin, P. New High Luminosity "Double Toroidal" Electron Spectrometer. *Rev. Sci. Instrum.* **1997**, *68*, 3728–3737.

(41) Le Guen, K.; Céolin, D.; Guillemin, R.; Miron, C.; Leclercq, N.; Bougeard, M.; Simon, M.; Morin, P.; Mocellin, A.; Burmeister, F. et al. Development of a Four-element Conical Electron Lens Dedicated to High Resolution Auger Electron–ion(s) Coincidence Experiments. *Rev. Sci. Instrum.* **2002**, *73*, 3885–3894.

(42) Céolin, D.; Miron, C.; Simon, M.; Morin, P. Auger Electron–ion Coincidence Studies to probe Molecular Dynamics. *J. Electron Spectrosc. Relat. Phenom.* **2004**, *141*, 171–181.

(43) Liu, X.-J.; Nicolas, C.; Robert, E.; Miron, C. EPICEA: Probing High-Energy Electron Emission In The Molecular Frame. *J. Phys.: Conf. Ser.* **2014**, *488*, 142005.

(44) Liu, X.-J.; Nicolas, C.; Miron, C. Design of a Lens Table for a Double Toroidal Electron Spectrometer. *Rev. Sci. Instrum.* **2013**, *84*, 033105.

(45) Travnikova, O.; Børve, K. J.; Patanen, M.; Söderström, J.; Miron, C.; Sæthre, L. J.; Mårtensson, N.; Svensson, S. The ESCA Molecule—Historical Remarks and New Results. *J. Electron Spectrosc. Relat. Phenom.* **2012**, *185*, 191–197.

(46) Siegbahn, K. Electron Spectroscopy for Atoms, Molecules, and Condensed Matter. *Rev. Mod. Phys.* **1982**, *54*, 709–728.

(47) Lestard, M. E. D.; Tuttolomondo, M. E.; Wann, D. A.; Robertson, H. E.; Rankin, D. W. H.; Ben Altabef, A. Experimental and Theoretical Structure and Vibrational Analysis of Ethyl Trifluoroacetate, $CF_3CO_2CH_2CH_3$. *J. Raman Spectrosc.* **2010**, *41*, 1357–1368.

(48) Schmidt, M. W.; Baldridge, K. K.; Boatz, J. A.; Elbert, S. T.; Gordon, M. S.; Jensen, J. H.; Koseki, S.; Matsunaga, N.; Nguyen, K. A.; Su, S. et al. General Atomic and Molecular Electronic Structure System. *J. Comput. Chem.* **1993**, *14*, 1347–1363.

(49) Hao, Y.; Inhester, L.; Hanasaki, K.; Son, S.-K.; Santra, R. Efficient Electronic Structure Calculation for Molecular Ionization Dynamics at High X-ray Intensity. *Struct. Dyn.* **2015**, *2*, 041707.

(50) Inhester, L.; Hanasaki, K.; Hao, Y.; Son, S.-K.; Santra, R. X-ray Multiphoton Ionization Dynamics of a Water Molecule Irradiated by an X-ray Free-electron Laser Pulse. *Phys. Rev. A* **2016**, *94*, 023422.

(51) Hehre, W. J.; Ditchfield, R.; Pople, J. A. Self-Consistent Molecular Orbital Methods. XII. Further Extensions of Gaussian-Type Basis Sets for Use in Molecular Orbital Studies of Organic Molecules. *J. Chem. Phys.* **1972**, *56*, 2257–2261.

(52) Hariharan, P. C.; Pople, J. A. The Influence of Polarization Functions on Molecular Orbital Hydrogenation Energies. *Theor. Chim. Acta* **1973**, *28*, 213–222.

(53) Sun, Q. Libcint: An Efficient General Integral Library for Gaussian Basis Functions. *J. Comput. Chem.* **2015**, *36*, 1664–1671.

(54) Fink, R. Theoretical Autoionization Spectra of $1s \rightarrow \pi^*$ Excited N_2 and N_2O. *J. Electron Spectrosc. Relat. Phenom.* **1995**, *76*, 295–300.

(55) Son, S.-K.; Young, L.; Santra, R. Impact of Hollow-atom Formation on Coherent X-ray Scattering at High Intensity. *Phys. Rev. A* **2011**, *83*, 033402.

(56) Mayer, I. Charge, Bond Order and Valence in the ab-initio SCF Theory. *Chem. Phys. Lett.* **1983**, *97*, 270–274.